Chemical Science

ROYAL SOCIETY OF CHEMISTRY

EDGE ARTICLE

View Article Online
View Journal | View Issue

Cite this: *Chem. Sci.*, 2025, **16**, 17287

All publication charges for this article have been paid for by the Royal Society of Chemistry

Received 26th June 2025
Accepted 15th August 2025

DOI: 10.1039/d5sc04720j

rsc.li/chemical-science

Macrocycles composed of biphenylene and butadiyne units with antiaromatic character

Shoko Nagayama,[a] Hiroki Kawakatsu,[a] Daisuke Asai,[a] Takumi Yokoyama,[a] Masahiro Yamashina,[b] Shinji Toyota[b] and Kazukuni Tahara[*a]

Herein, we report the synthesis and characterization of π-conjugated macrocycles, with diameters over 2.4 nanometers, composed of biphenylene and butadiyne units. Specifically, biphenylene-2,7-diyl-butadiyne-1,4-diyl (BB) macrocycles were synthesized *via* the intermolecular Hay coupling reaction of a 2,7-diethynylbiphenylene derivative. The BB macrocycles exhibited absorption bands extending up to ~600 nm and emitted red luminescence. Moreover, scanning tunneling microscopy observations revealed that the BB macrocycles formed self-assembled molecular networks at the liquid–graphite interface, showing higher tunneling efficiency. The BB macrocycles exhibited high energy levels of the highest occupied molecular orbitals and narrow energy gaps due to the elongated π-electron conjugation through the biphenylene units. Theoretically predicted responses to an external magnetic field using quantum chemical calculations of BB macrocycle models revealed reinforced antiaromatic character at four-membered rings. The present information will advance the structural design and property tuning of macrocyclic compounds with antiaromatic character.

Introduction

π-Conjugated, shape-persistent macrocyclic compounds are of great interest because of their fundamental synthetic and theoretical aspects, as well as their applications in optoelectronic materials, hierarchical molecular architecture construction *via* self-assembly in various environments, and guest recognition at intrinsic pore or cavity space.[1–7] Over the past half-century, different macrocycles, such as planar two-dimensional (2D) molecular rings and three-dimensional (3D) molecular hoops and belts, have been produced based on sophisticated molecular design.[8–11] Rigid π-electron conjugated units such as benzene, polycyclic aromatics, and heterocyclic rings, as well as porphyrin, oligophenyl, ethylene, butadiene, ethyne, and butadiyne units, are essential components for the construction of such macrocycles. In particular, aromatic units or those combined with linear carbon–carbon triple bond units are typically employed because of their rigidity and stability. However, macrocycles incorporating an antiaromatic component remain scarce. Esser and coworkers recently reported molecular hoops comprising dibenzopentalene units, which exhibited unique optoelectronic characteristics because of the antiaromatic pentalene units.[12,13] Moreover, there are few examples of nanometer-scale macrocyclic molecules with global antiaromatic character. Anderson and coworkers demonstrated that the tetra-cation and tetra-anion of a six-porphyrin nanoring template complex with 80-π and 88-π electrons were antiaromatic based on their ring current effects under an external magnetic field.[14–16] Furthermore, tetraradicaloid macrocycles have been reported to show antiaromatic character.[17–19] Nevertheless, further fundamental studies on macrocycles with antiaromatic character are required to gain an in-depth understanding of the structure–property relationships. Such insights are crucial for tuning their properties, including the modulation of highest occupied molecular orbital (HOMO)–lowest unoccupied molecular orbital (LUMO) energy levels and their energy gaps,[20–22] as well as the formation of molecular stacks *via* antiaromatic units,[23–25] which are key elements for prospective applications in optoelectronic materials and the design of self-assembled structures.

π-Conjugated ring units are essential building blocks in the design of π-conjugated macrocycles because they link other units with a tunable connection angle.[26] For instance, a benzene ring offers 60° (*ortho*), 120° (*meta*), and 180° (*para*) connections (Fig. 1a). Notably, the efficiency of π-electron system elongation differs by position: it is efficient in the *ortho*- and *para*-positions but not in the *meta*-position.[27–32] Polycyclic aromatic units (*i.e.*, naphthalene, anthracene, phenanthrene, and pyrene units) and oligophenyl units (*i.e.*, biphenyl, terphenyl, and quaterphenyl units) share geometric and electronic features as the molecular linkers. For heterocyclic rings, a pyridine ring has similar features to the benzene ring,[33,34] whereas a thiophene ring extends the π-electron system efficiently at the α-position (2-

[a]*Department of Applied Chemistry, School of Science and Technology, Meiji University, 1-1-1 Higashimita, Tama-ku, Kawasaki, Kanagawa, 214-8571, Japan. E-mail: tahara@meiji.ac.jp*

[b]*Department of Chemistry, School of Science, Institute of Science Tokyo, 2-12-1 Ookayama, Meguro-ku, Tokyo 152-8551, Japan*

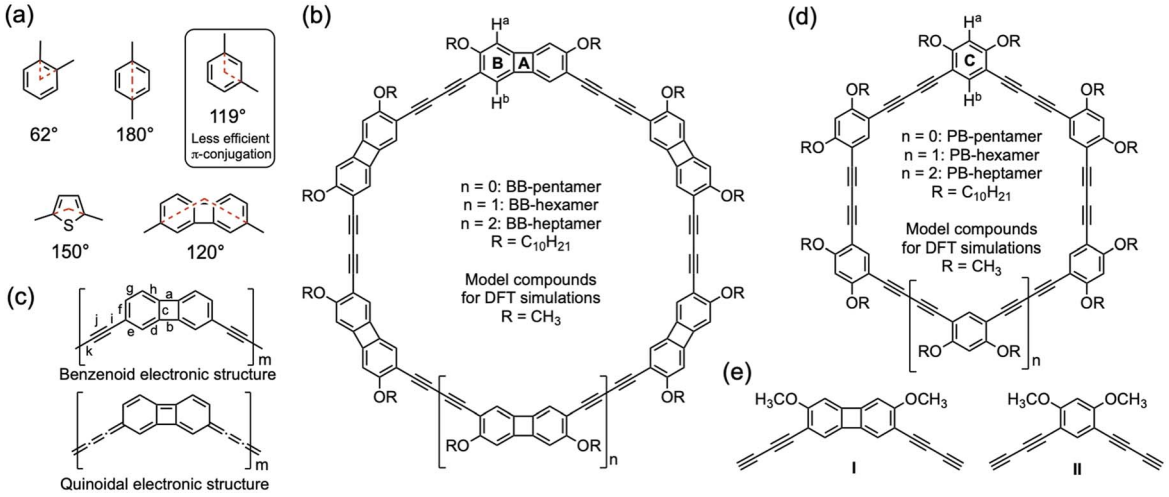

Fig. 1 Chemical structures of representative molecular linker units: benzene, thiophene, and biphenylene units. The angles between the two $C(sp^2)$–$C(CH_3)$ bonds in the linker units derived from the density functional theory (DFT) (B3LYP/6-311G(d,p))-optimized geometries of the corresponding dimethyl-substituted compounds (Fig. S1). (b) Chemical structures of the BB macrocycles: BB-pentamer, BB-hexamer, and BB-heptamer. The capital letters A and B indicate 4 MRs and six-membered rings (6 MRs). (c) Selected electronic structures of the BB macrocycles: benzenoid (top) and quinoidal (bottom) electronic structures. Small alphabetic letters a–k in the benzenoid electronic structure (top) indicate the bond positions. A quinoidal electronic structure (bottom) contributes to an increase in the local antiaromatic character at the 4 MR (Fig. S15). (d) Chemical structures of the PB macrocycles: PB-pentamer, PB-hexamer, and PB-heptamer. The capital letter C indicates the 6 MR. (e) Chemical structures of model compounds **I** and **II** for the DFT simulations.

and 5-positions) by ~150°.[35,36] Although there are many examples of molecular linker units, those connected to other units at an angle of 120° (equivalent to the *meta*-position) with good π-electron elongation efficiency are few,[37,38] which limits the production of fully π-conjugated, planar macrocycles. Employing such a molecular linker unit is expected to develop structural design and to enhance their optoelectronic properties.

In this context, we report the synthesis and properties of π-conjugated, planar macrocycles, with diameters over 2.4 nanometers, comprising biphenylene units with weak antiaromatic character and butadiyne units as spacers (Fig. 1b and c). To our knowledge, the biphenylene unit has not yet been used to produce π-conjugated macrocycles with diameters over a few nanometers. The optoelectronic properties in solution and electron tunneling efficiency on a solid surface confirmed the formation of π-electron conjugated systems through the biphenylene units in biphenylene-2,7-diyl-butadiyne-1,4-diyl (BB) macrocycles, which showed smaller HOMO–LUMO gaps

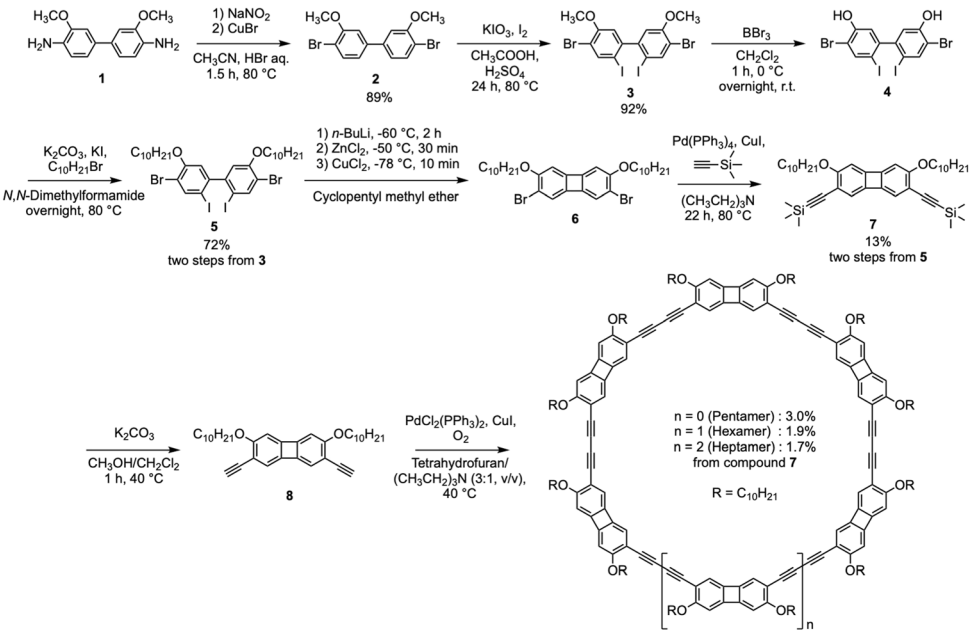

Scheme 1 Synthesis of the BB macrocycles.

with higher local antiaromatic character at the four-membered rings (4 MRs), based on the comparison with non-cyclic reference compounds and a 1,3-phenylene-butadiyne-1,4-diyl (PB) macrocycle (Fig. 1d and e).

Results and discussion

Design of BB and PB macrocycles

Biphenylene, a polycyclic hydrocarbon with two aromatic 6 MRs and an antiaromatic 4 MR, was chosen as a molecular building block for the target macrocycles.[39] The π-electrons at the 6 MRs inhibit fused bonds, reducing the antiaromatic character of the 4 MR in biphenylene.[40–43] Biphenylene has recently been the subject of interest because it is the smallest unit of the biphenylene network.[44] A unique feature of biphenylene as a molecular linker is π-electron elongation at the 2- and 7-positions with a connection angle of ∼120° (equivalent to the *meta*-position).[37,38] Thus, we delineated that planar, π-conjugated macrocycles can be produced by connecting this unique molecular linker at the 2- and 7-positions. Moreover, we predicted that the contribution of a quinoidal electronic structure would reinforce the antiaromatic nature of the 4 MRs in such biphenylene macrocycles (Fig. 1c and S15).[45–47] A butadiynylene unit was chosen as a spacer unit to prevent steric repulsion of the biphenylene units.[48] Indeed, using quantum chemical calculations at the B3LYP/6-311G(d,p) level of theory, geometry optimization of the models of BB macrocycles with methoxy groups predicted that the BB-pentamer and BB-hexamer adopt planar geometries with D_{5h} and D_{6h} symmetry constraints (Fig. S2). On the other hand, the BB-heptamer has a shallow saddle-type geometry without a symmetry constraint (Fig. S3). The diameters of the BB-pentamer, BB-hexamer, and BB-heptamer are 2.4, 2.9, and 3.6 nm, respectively. Two decyloxy groups were introduced into each biphenylene unit to ensure their solubility in common organic solvents. As references, we also designed PB macrocycles featuring benzene rings instead of biphenylene units with the same substituent groups (Fig. 1d and S4).

Synthesis of BB and PB macrocycles

The synthesis of the BB macrocycles is outlined in Scheme 1. Commercially available biphenyl derivative **1** was transformed to dibromide **2** *via* the bromination of an *in situ*-generated diazonium salt. The iodination of **2** produced diiodide **3**. Methoxy groups of **3** were replaced with decyloxy groups *via* the deprotection and alkylation of hydroxy groups to afford compound **5**. The construction of the 4 MR was performed *via* a copper–zinc catalyzed intramolecular coupling reaction of **5** to produce 2,7-dibromo-3,6-bis(decyloxy)biphenylene **6**. The Sonogashira–Hagiwara coupling reaction of **6** with (trimethylsilyl)acetylene followed by a desilylation reaction of **7** produced monomer **8**. The intermolecular Hay coupling reaction of **8** in the presence of palladium and copper catalysts

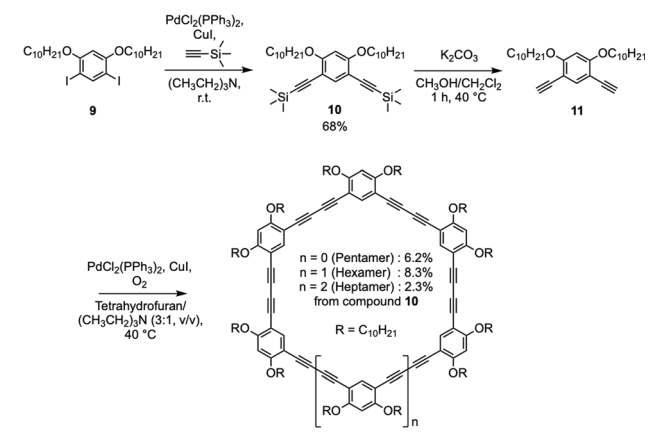

Scheme 2 Synthesis of the PB macrocycles.

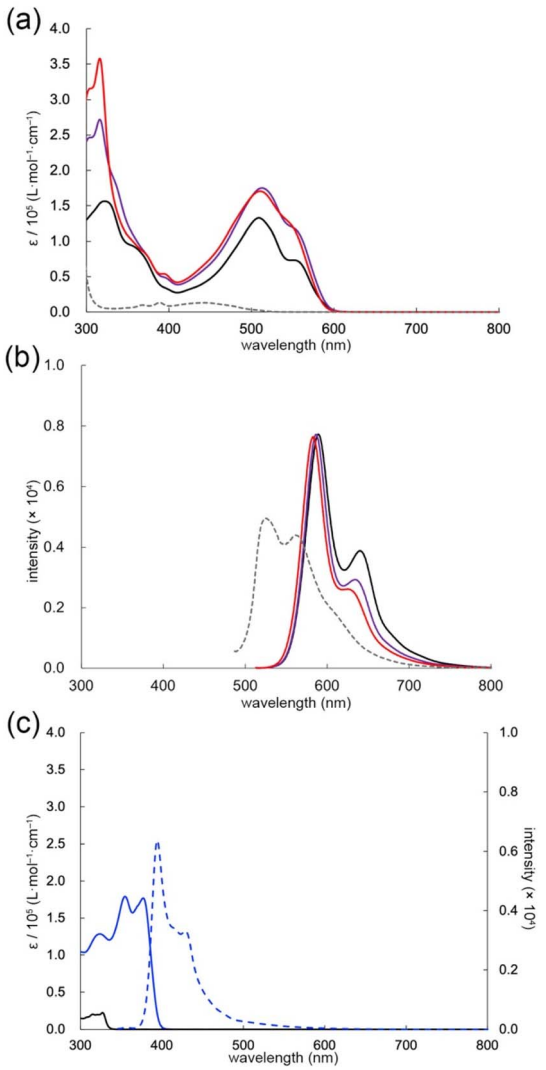

Fig. 2 (a and b) UV-vis absorption (a) and emission (b) spectra of the BB-pentamer (black line), BB-hexamer (purple line), BB-heptamer (red line), and compound **7** (gray dotted line). The excitation wavelengths were 500 (BB macrocycles) and 445 nm (compound **7**). (c) UV-vis absorption and emission spectra of the PB-hexamer (blue and blue dotted lines) and compound **10** (black line). The excitation wavelength was 320 nm (PB-hexamer). In the emission spectra, emission bands do not reflect their intrinsic intensities because we used different sensitivity settings of the spectrometer for each measurement. All spectra were measured in *o*-dichlorobenzene at room temperature except for compound **10** (dichloromethane).

under highly dilute conditions (6.7×10^{-3} mol L^{-1}) produced various oligomeric products. Careful separation of the crude reaction mixture using recycling preparative high-performance liquid chromatography provided three products as red solids. Simple signal patterns in the proton (^1H) and carbon-13 (^{13}C) nuclear magnetic resonance (NMR) spectra of these products in deuterated chloroform ($CDCl_3$) at room temperature confirmed their highly symmetric structures in solution. The doubly-charged molecular ions (M^{2+}) of these products detected using electrospray ionization time-of-flight mass spectroscopy confirmed the formation of the cyclic BB-pentamer (*m*/*z*: 1275.8716), BB-hexamer (*m*/*z*: 1531.0449), and BB-heptamer (*m*/*z*: 1786.2223). The BB-pentamer, BB-hexamer, and BB-heptamer were obtained in yields of 3.0%, 1.9%, and 1.7% respectively, from compound **7**.

The PB macrocycle reference compounds were synthesized using similar synthetic protocols starting from 1,5-bis(decyloxy)-2,4-diiodobenzene (**9**) (Scheme 2). The intermolecular coupling of 1,5-bis(decyloxy)-2,4-diethynylbenzene (**11**) after the removal of the trimethylsilyl group of **10** afforded the cyclic PB-pentamer, PB-hexamer, and PB-heptamer in 6.2%, 8.3%, and 2.3% from compound **10**. Detailed synthetic procedures are provided in the SI.

Electronic properties

The absorption and luminescence spectra of the macrocycles in *o*-dichlorobenzene at room temperature are shown in Fig. 2, and the spectroscopic data are summarized in Table 1. All BB macrocycles exhibited two broad absorption bands with maxima at ~320 and 510 nm. Because HOMO–LUMO transitions are forbidden for all BB macrocycles, the longer wavelength bands were attributed to HOMO–LUMO+1 and HOMO−1–LUMO transitions for the BB-pentamer and BB-hexamer and HOMO–LUMO+1, HOMO–LUMO+2, HOMO−1–LUMO, and HOMO−2–LUMO for the BB-heptamer, as supported by the time-dependent (TD)-DFT calculations of the corresponding model compounds having methoxy groups at the B3LYP/6-311+G(d,p) level of theory (Fig. S7–S9 and Tables S3–S5). The absorption onsets were 611, 603, and 600 nm for the BB-pentamer, BB-hexamer, and BB-heptamer, and the estimated optical band gaps were 2.03, 2.06, and 2.07 eV, respectively (Fig. S16). There were no substantial differences in the absorption maxima and onsets among macrocycles based on size. This may indicate an effective conjugation length based on the comparison with linear model compounds (Fig. S6 and Table S2).[50] The absorption maxima and onsets were red-shifted relative to those of acyclic compound **7** (maximum: 443 nm, onset: 540 nm). All BB macrocycles showed red luminescence. In the emission spectra, the BB macrocycles exhibited emission bands showing maxima at 589, 587, and 583 nm and quantum yields of 0.21, 0.24, and 0.22 for the BB-pentamer, BB-hexamer, and BB-heptamer, respectively. Likewise, the emission bands were red-shifted, and the quantum yields were higher compared to compound **7** (maximum: 525 nm, quantum yield: 0.04). The PB-hexamer and corresponding acyclic compound **10** showed absorption bands with maxima of 377 and 327 nm and onsets of 401 and 342 nm, respectively. The PB-hexamer emitted weak blue luminescence with an emission maximum of 395 nm and a quantum yield of 0.03.

Differential pulse voltammetry measurements of the macrocycles were conducted at room temperature using a solution of the macrocycle in *o*-dichlorobenzene (2.0×10^{-4} mol L^{-1}) with tetrabutylammonium hexafluorophosphate as the supporting electrolyte (Fig. S17–S19). The potential was calibrated against an oxidation wave of ferrocene. Broad oxidation waves were observed at anodic peak potentials (E_{ap}) of 0.15, 0.16, and 0.63 V for the BB-pentamer, BB-hexamer, and PB-hexamer, respectively. No reduction waves were observed until −1.7 V for all macrocycles in our experimental conditions. The lower oxidation potentials of the BB macrocycles were ascribed to their higher HOMO energy levels because of their electron-rich nature.

π-Electron conjugated systems of macrocycles

The red shifting in the absorption onsets was caused by the cyclization of the biphenylene system, indicating that the

Table 1 Summary of the ultraviolet-visible (UV-vis) absorption and emission spectra for the BB and PB macrocycles, as well as reference compounds **7** and **10** in *o*-dichlorobenzene at room temperature, and DFT-predicted HOMO–LUMO energy gaps[a]

Compound	Absorption maxima (nm)	Absorption onset[b] (nm)	Optical band gap[c] (eV)	DFT-predicted HOMO–LUMO energy gap[d] (eV)	Emission maximum (nm)	Emission quantum yield[e]
BB-pentamer	322, 509, 551	611	2.03	2.10	589	0.21
BB-hexamer	316, 513, 541	603	2.06	2.09	587	0.24
BB-heptamer	316, 510, 547	600	2.07	2.18	583	0.22
7	294, 443	540	2.30	—[f]	525	0.04
PB-hexamer	355, 377	401	3.09	3.42	429	0.03
10	293, 327	342	3.63	—[f]	—[g]	—[g]

[a] *o*-Dichlorobenzene was used as the solvent except for compound **10** (dichloromethane) because of the limited solubility of the BB-hexamer in conventional organic solvents. [b] Gaussian deconvolution was applied for each absorption spectrum (Fig. S16). The onset wavelength was estimated as the wavelength at which the Gaussian curve at the longest wavelength reaches 2% of its maximum. [c] Optical bandgaps were derived from the absorption onsets. In the present macrocycles, these values do not correspond to the HOMO–LUMO gaps as the HOMO–LUMO transitions are forbidden. [d] Calculated using the model compounds at the B3LYP/6-311G(d,p) level of theory. [e] Absolute emission quantum yields. [f] Not calculated. [g] No emission was observed.

Table 2 Wiberg bond indices (WBI) and bond lengths of the model compounds of the BB and PB macrocycles and reference compound I

Compound	WBI and bond length[a]										
	Bond a	Bond b	Bond c	Bond d	Bond e	Bond f	Bond g	Bond h	Bond i	Bond j	Bond k
BB-pentamer	1.025 (1.509 Å)	1.002 (1.514 Å)	1.230 (1.431 Å)	1.506 (1.368 Å)	1.255 (1.438 Å)	1.310 (1.418 Å)	1.312 (1.421 Å)	1.460 (1.376 Å)	1.155 (1.415 Å)	2.481 (1.228 Å)	1.267 (1.353 Å)
BB-hexamer	1.026 (1.497 Å)	1.002 (1.508 Å)	1.231 (1.421 Å)	1.506 (1.365 Å)	1.256 (1.431 Å)	1.307 (1.418 Å)	1.313 (1.417 Å)	1.458 (1.373 Å)	1.156 (1.410 Å)	2.480 (1.218 Å)	1.267 (1.352 Å)
BB-heptamer[b]	1.025 (1.497 Å)	1.002 (1.509 Å)	1.231–1.232 (1.420 Å)	1.504–1.505 (1.365 Å)	1.257–1.259 (1.431 Å)	1.307–1.309 (1.417–1.418 Å)	1.311–1.312 (1.417 Å)	1.458–1.459 (1.372 Å)	1.151–1.155 (1.410–1.411 Å)	2.481–2.485 (1.218 Å)	1.262–1.266 (1.352–1.353 Å)
I	1.022 (1.500 Å)	1.002 (1.507 Å)	1.234 (1.420 Å)	1.502 (1.365 Å)	1.261 (1.430 Å)	1.314 (1.416 Å)	1.306 (1.418 Å)	1.466 (1.372 Å)	1.144 (1.423 Å)	2.522 (1.215 Å)	1.231 (1.360 Å)
PB-hexamer	—	—	1.248 (1.417 Å)	1.363 (1.400 Å)	1.363 (1.400 Å)	1.248 (1.417 Å)	1.373 (1.396 Å)	1.373 (1.396 Å)	1.131 (1.415 Å)	2.512 (1.216 Å)	1.211 (1.355 Å)

[a] Bond length is in parenthesis. [b] Bond indices ranges and bond length ranges are presented for some bonds due to the lower symmetric geometry of the BB-heptamer.

biphenylene unit acts as a π-conjugated linker of ~120° at the 2- and 7-positions, yet the elongation of the π-electron conjugated system reaches saturation by five repeating units (Table S2). The absorption onsets of other planar macrocycles comprising aromatic ring(s) and butadiynylene or ethynylene linkers have been reported to be <450 nm,[51–55] except for macrocycles comprising the thiophene unit.[36] According to the quantum chemical calculations of the model compounds of the BB macrocycles, the predicted HOMO–LUMO gaps are 2.09–2.18 eV (Table 1). Notably, the predicted HOMO–LUMO gap of the BB-hexamer is narrower than those of the corresponding virtual naphthalene-2,7-diyl-butadiyne-1,4-diyl hexamer and anthracene-2,7-diyl-butadiyne-1,4-diyl hexamer (3.23 and 2.73 eV), though the π-electron number of biphenylene (12-π) is inbetween those of naphthalene (10-π) and anthracene (14-π) (Fig. S5 and Table S1). These facts support the substantial reduction in the HOMO–LUMO gaps for the BB macrocycles.

The Wiberg bond indices (WBI)[56] analysis based on natural bonding orbital and localized orbital locator (LOL-π) analysis[57,58] were performed for the BB macrocycles and reference model compound **I** (Fig. 1c) to identify the bonding nature and degree of π-electron (de)localization at each bond. In the BB macrocycles, the WBI values of bonds a, d, g, i, and k were greater than those of reference compound **I**, whereas those of bonds f, h, and j were lower (Table 2). The LOL-π analyses confirmed greater π-electron densities for outer bonds a over inner bonds b in the BB macrocycles (Fig. 3a and S10). The bond lengths of these compounds were qualitatively consistent with the aforementioned features. These analyses indicate the contribution of a quinoidal electronic structure in the BB macrocycles.

Local (anti)aromaticity of macrocycles

The chemical shift values of hydrogen atoms attached to aromatic or antiaromatic rings in the ^{1}H NMR spectra provide experimental evidence for the induced ring current effect. In the ^{1}H NMR spectra of the BB-pentamer, BB-hexamer, and BB-heptamer, the outer hydrogens (H^a) resonated at 6.41, 6.42, and 6.42 ppm, respectively, and the inner hydrogens (H^b) resonated at 6.66, 6.63, and 6.61 ppm, respectively. H^a and H^b appeared at 6.43 and 6.60 ppm for compound **8**, 6.33 and 7.60 ppm for the PB-hexamer, and 6.34 and 7.51 ppm for compound **11**, respectively. The slight increase in the magnetic shielding effect for H^a relative to the corresponding acyclic compounds indicated the weak attenuation of diatropic ring currents in the 6 MRs upon macrocyclization. The downfield shifts in H^b for the macrocycles, particularly for the BB-pentamer, would be ascribed to in-plane induced ring currents at the inner periphery.[59,60]

To further investigate the local aromaticity of each ring, we performed nucleus-independent chemical shift (NICS) calculation.[61] We used the NICS(1)$_{zz}$ value, which is the *zz* component of the isotropic NICS value calculated at 1 Å above the ring centers.[62] The NICS values at 4 MRs A were all positive, and those for the BB macrocycle models were slightly higher than those acyclic model compound **I** (Table 3). Conversely, the NICS

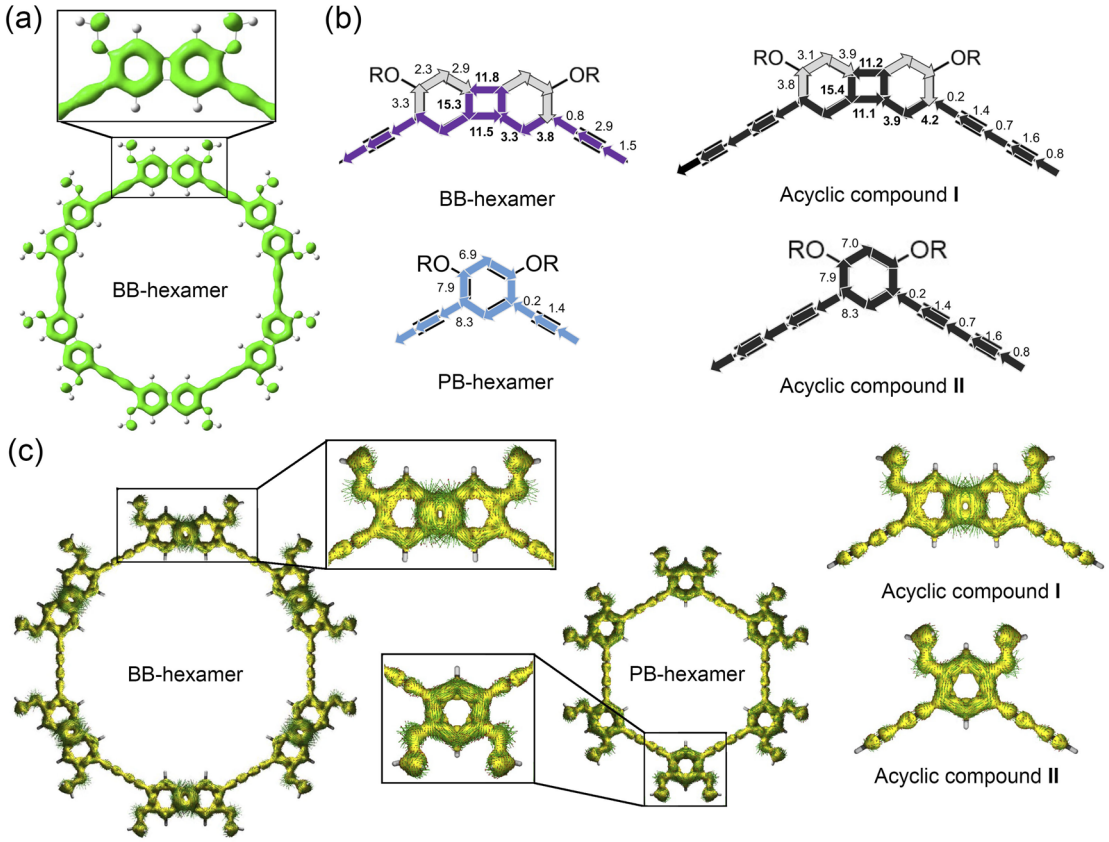

Fig. 3 (a) LOL-π analysis of the model of the BB-hexamer (isovalue: 0.363). (b) Gauge-including magnetically induced current (GIMIC) analyses of the models of the BB-hexamer and PB-hexamer, compound **I**, and compound **II** (R = methyl group). The current paths are represented by arrows, and their strengths are given in nA/T. (c) Anisotropy of the induced current density (AICD)-π plots of the model of the BB-hexamer. All calculations were conducted at the B3LYP/6-311G(d,p) level of theory employing the gauge-independent atomic orbital (GIAO) method. The LOL-π analyses, GIMIC analyses, and AICD-π plots of the models of the BB-pentamer and BB-heptamer and in-plane AICD-π plots of the models of the BB-hexamer and PB-hexamer are shown in the SI (Fig. S10–S14).

Table 3 The NICS(1)$_{zz}$ values of the model compounds of the BB and PB macrocycle, as well as reference compounds **I** and **II** calculated using the GIAO method at the B3LYP/6-311G(d,p) level of theory

	NICS(1)$_{zz}$ value[a] (ppm)		
Compound	4 MR A	6 MR B	6 MR C
BB-pentamer	35.1	−7.8	—
BB-hexamer	34.8	−7.9	—
BB-heptamer[b]	34.8	−8.1	—
I	34.4	−8.7	—
PB-hexamer	—	—	−9.2
II	—	—	−9.4

[a] Calculated at the 1 Å above the ring centroid. [b] Average values of seven rings because of its nonplanar geometry.

values at 6 MRs B were all negative, with the values for the BB macrocycle model being larger than that for compound **I**. The paratropic ring currents at the 4 MRs strengthened, whereas the diatropic ring currents at the 6 MRs weakened. There is the small difference in the NICS values between the PB macrocycle and acyclic compound **II** (Fig. 1e) in 6 MRs C. Next, the magnetically induced current strengths and the current densities were calculated using the gauge-including magnetically induced current (GIMIC) method.[63,64] Clockwise (paratropic) and counter-clockwise (diatropic) currents flowed at 4 MRs A and 6 MRs B in the BB macrocycles (Fig. 3b and S12), and diatropic currents flowed at 6 MRs C in the PB-hexamer.[65] Moreover, the diatropic current strengths in 6 MRs B of the BB macrocycles were weaker than those of acyclic compound **I**. There was almost no difference in 6 MRs C between the PB macrocycle and acyclic compound **II**. In the 4 MRs, the current strengths of bonds a and b were higher in the BB macrocycles than acyclic compound **I**, whereas the current strengths of bond c were nearly identical, indicating slightly stronger overall paratropic ring currents for the BB macrocycles. The anisotropy of the induced current density (AICD) analyses of the BB and PB macrocycles for the out-of-plane π-electrons also qualitatively agreed with the GIMIC analyses (Fig. 3c and S13).[66,67]

All magnetic shielding calculations supported higher antiaromaticity at the 4 MRs and lower aromaticity at the 6 MRs for the BB macrocycles compared to the acyclic reference compound.

Self-assembly of macrocycles at the liquid–graphite interfaces

Planar π-electron conjugated macrocycles may spontaneously form self-assembled molecular networks (SAMNs)[68] with

various topologies and functionalities at the liquid–solid interface.[69–72] Rigid polygonal macrocycles are essential building blocks for the advancement of 2D crystal engineering.[49,73,74] SAMNs are typically observed at submolecular resolution using scanning tunneling microscopy (STM).[75] Moreover, the STM technique can reveal the molecular electronic properties. In this context, we investigated the self-assembly of the present macrocycles at the interface. A solution of the BB macrocycle in 1,2,4-trichlorobenzene (TCB) at concentrations ranging from 1.0×10^{-6} to 2.0×10^{-4} mol L^{-1} was dropped onto highly oriented pyrolytic graphite. The SAMNs were observed using STM at the TCB-graphite interface at room temperature.

Fig. 4 shows the self-assembly of the BB-hexamer at the TCB-graphite interface. The bright cyclic features correspond to π-conjugated systems of the BB-hexamer because of its high tunneling efficiency (Fig. 4a and b), confirming a nanometer-scale macrocyclic structure.[76] At a low solute concentration (1.0×10^{-6} mol L^{-1}), the molecules formed a hexagonally aligned monolayer, reflecting the planar hexagonal geometry (Fig. 4c). The decyloxy chains that run parallel to the main symmetry axes of graphite should occupy a darker area.[77] These chains interdigitated each other, maximizing van der Waals interactions and acting as intermolecular linkages.

Notably, increasing the solute concentration to 1.0×10^{-5} mol L^{-1} led to multilayer formation *via* epitaxial structural growth (Fig. 4d and e). The brighter cycles correspond to top-layer molecules, as supported by the cross-sectional analysis (Fig. 4f), and the macrocycles favor offset arrangements (Fig. 4g). Though the epitaxial structural growth from the monolayer has been reported for the disk-shaped molecules at the liquid–solid interfaces,[78–81] the present observation for the macrocycle with the large intrinsic pore is intriguing in view of the production of porous multi-layered films on surface.

The BB-pentamer and BB-heptamer also produced SAMNs at the TCB-graphite interface. Because pentagons and heptagons cannot tessellate, these molecules formed quasi-hexagonal structures by deforming their intrinsic polygonal shapes (Fig. S20 and S21).[49,73,74] The details are summarized in the SI. Neither molecule exhibited epitaxial structural growth even at high solute concentrations of 1.1×10^{-4} (pentamer) and 2.0×10^{-4} mol L^{-1} (heptamer). The quasi-hexagonal patterns of the distorted BB-pentamer and BB-heptamer, which differ from the hexagonal arrangement of the BB-hexamer, changed the interlayer interactions, leading to no epitaxial film growth.

The PB-hexamer aligned in a quasi-hexagonal manner, forming linear molecular rows in which one alkoxy chain per molecule oriented to a liquid phase (Fig. 5a–c). No multilayer formation was observed throughout a wide concentration range (1.0×10^{-6} to 2.0×10^{-4} mol L^{-1}).

To address the difference in the electronic properties of the macrocycles, SAMN formation in a mixture of the BB-hexamer and PB-hexamer at low concentrations of 5.1×10^{-7} mol L^{-1} and 1.5×10^{-6} mol L^{-1} was investigated. Both molecules

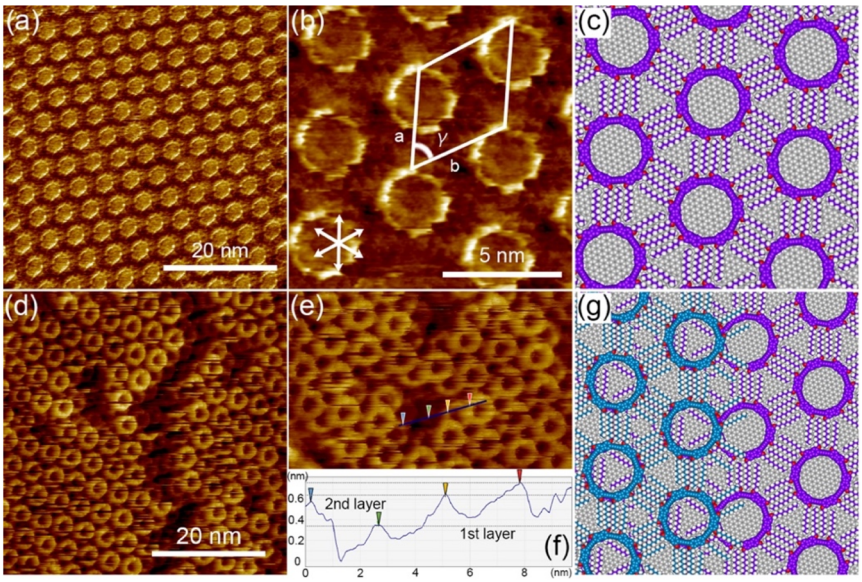

Fig. 4 STM images and network models of SAMNs formed by the BB-hexamer at the TCB-graphite interface. (a) Large and (b) digitally-zoomed small area STM images of monolayers formed at a low solute concentration (1.0×10^{-6} mol L^{-1}) and (c) corresponding network model on a graphene bilayer sheet optimized using a molecular mechanics (MM) simulation (COMPASS III force field). The unit cell parameters are $a = 4.3 \pm 0.1$ nm, $b = 4.3 \pm 0.1$ nm, and $\gamma = 60.1 \pm 0.4°$. White arrows in (b) indicate the directions of the main symmetry axes of the underlying graphite. (d) Large and (e) small area STM images of multilayers formed at a high solute concentration (1.0×10^{-5} mol L^{-1}) and (g) corresponding MM-optimized network model of the multilayer (offset model) on a graphene bilayer sheet. The macrocyclic and network pores are most likely filled with the solvent molecules (Fig. S22). In (g), the molecules in the second layer were omitted for clarity on the right side of the model. (f) Apparent height analysis along a blue line in (e). The tunneling parameters are $I_{set} = 150$ pA, $V_{bias} = -0.69$ V for (a), $I_{set} = 150$ pA, $V_{bias} = -0.85$ V for (b), $I_{set} = 150$ pA, $V_{bias} = -0.90$ V for (d), and $I_{set} = 150$ pA, $V_{bias} = -0.90$ V for (e). Color code for atoms in the MM models (c and g), purple: carbon atoms of the BB-hexamer (first layer), turquoise blue: carbon atoms of the BB-hexamer (second layer), gray: carbon atoms of the graphene bilayer sheet, red: oxygen atoms, and white: hydrogen atoms.

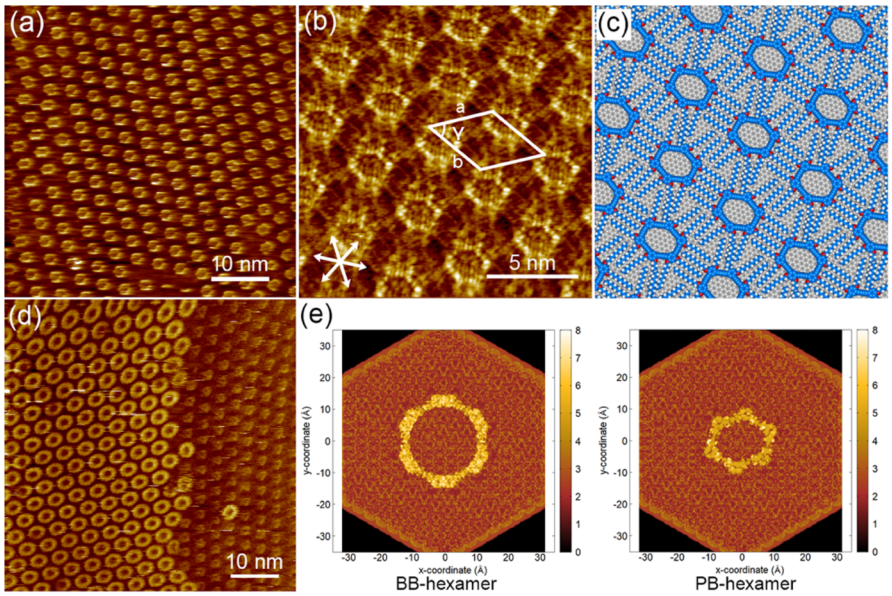

Fig. 5 (a–c) STM images and network models of SAMNs formed by the PB-hexamer at the TCB-graphite interface. (a) Large and (b) small area STM images of monolayers formed at a low solute concentration (1.0×10^{-6} mol L^{-1}). The unit cell parameters are $a = 3.8 \pm 0.1$ nm, $b = 3.7 \pm 0.1$ nm, and $\gamma = 59.2 \pm 0.8°$. The white arrows in (b) indicate the directions of the main symmetry axes of the underlying graphite. (c) Network model on a graphene bilayer sheet optimized using an MM simulation (COMPASS III force field). (d) STM image of SAMN formed by a mixture of the BB-hexamer and PB-hexamer at the TCB-graphite interface (concentrations: 5.1×10^{-7} and 1.5×10^{-6} mol L^{-1}). (e) Simulated STM image of the models of the BB-hexamer and PB-hexamer on graphene in a constant current mode (1.00×10^{-4} a.u.) using the GFN2-*x*TB method ($V_{bias} = -1.100$ V). The *z*-axis indicates the distance between the STM tip and the graphene sheet (0 Å). The tunneling parameters are $I_{set} = 150$ pA, $V_{bias} = -1.10$ V for (a), $I_{set} = 150$ pA, $V_{bias} = -1.19$ V for (b), and $I_{set} = 150$ pA, $V_{bias} = -1.11$ V for (d). Color code for atoms in the MM models (c), aqua blue: carbon atoms of the PB-hexamer, gray: carbon atoms of the graphene bilayer sheet, red: oxygen atoms, and white: hydrogen atoms.

formed their intrinsic alignments as separated domains (Fig. 5d, S23, and S24).[82] Notably, the macrocyclic core of the BB-hexamer (left domain in Fig. 5d) appeared brighter than that of the PB-hexamer (right domain in Fig. 5d) at the same bias voltage (sample negative). To qualitatively verify the difference in image appearance, we theoretically simulated the STM images of the BB-hexamer and PB-hexamer on a graphene sheet under a constant current mode using the GFN2-xTB method (Fig. 5e and S25).[83,84] The simulated images confirmed that the BB-hexamer appears brighter (higher) than the PB-hexamer. This is related to the higher tunneling efficiency of the BB-hexamer because of its higher HOMO energy level,[85,86] supporting the electron-rich nature of the BB macrocycles containing the weakly antiaromatic 4 MRs.

Conclusions

In this study, we reported the production and properties of macrocycles, with diameters over 2.4 nanometers, comprising biphenylene and butadiyne units. The comparison of the BB macrocycles to the PB macrocycle and acyclic reference compounds in terms of their photophysical and electronic properties, together with the DFT calculations, demonstrated that the biphenylene unit acts as a linker with a connection angle of ~120°, maintaining π-electron conjugation, yet the elongation of the π-electron conjugated system reaches saturation among the BB macrocycles. The quinoidal electronic structure enhances the local antiaromatic character of the 4 MRs of the BB macrocycles, thereby influencing their electronic properties. The present findings are useful for advancing structural design and property tuning of macrocyclic compounds based on the molecular components exhibiting antiaromatic character. The self-assembly of the macrocycles at the liquid–solid interface offers sophisticated control over thin-film structures (monolayer *vs.* multilayer) while allowing the modulation of interfacial electronic properties. The unique properties of biphenylene-containing macrocycles may pave the way for advances in organic materials science.

Author contributions

S. N. and H. K. performed the synthesis and characterization. S. N. performed the STM observation of the macrocycles at the interfaces. S. N. and D. A. conducted the quantum chemical calculations. T. Y. performed the STM image simulations. M. Y. and S. T. organized the ESI-TOF mass analysis and commented on the manuscript. S. N. drafted the manuscript and prepared the figures and tables. K. T. conceived the idea, supervised the investigation, and wrote the manuscript. All authors discussed the results and approved the final manuscript.

Conflicts of interest

There are no conflicts to declare.

Data availability

The data supporting this article have been included as part of the SI.

Details of synthesis, details of quantum chemical calculations, additional STM images, details of MM calculations, ^{1}H and ^{13}C NMR spectra of new compounds, cartesian coordinates of DFT-optimized geometries. See DOI: **https://doi.org/10.1039/d5sc04720j**.

Acknowledgements

This work was supported by JSPS KAKENHI Grant Numbers JP20H02553, JP23K20271, and JP25K01602, Research Project Grant (B) by Institute of Science and Technology, Meiji University, Tokuyama Science Foundation, and Iketani Science and Technology Foundation. This work was performed under the Cooperative Research Program of "NJRC Mater. & Dev. (MEXT)". The authors thank Materials Analysis Division, Core Facility Center, Institute of Science Tokyo, for performing high-resolution mass (ESI-TOF) analysis.

References

1 M. Iyoda, J. Yamakawa and M. J. Rahman, Conjugated Macrocycles: Concepts and Applications, *Angew. Chem., Int. Ed.*, 2011, **50**, 10522.
2 C. Grave and A. D. Schlüter, Shape-Persistent, Nano-Sized Macrocycles, *Eur. J. Org Chem.*, 2002, 3075.
3 W. Zhang and J. S. Moore, Shape-Persistent Macrocycles: Structures and Synthetic Approaches form Arylene and Ethynylene Building Blocks, *Angew. Chem., Int. Ed.*, 2006, **45**, 4416.
4 Y. Xu and M. von Delius, The Supramolecular Chemistry of Strained Carbon Nanohoops, *Angew. Chem., Int. Ed.*, 2020, **59**, 559.
5 S. Höger, Shape-Persistent Macrocycles: From Molecules to Materials, *Chem.–Eur. J.*, 2004, **10**, 1320.
6 A. H. Flood, Creating Molecular Macrocycles for Anion Recognition, *Beilstein J. Org. Chem.*, 2016, **12**, 611.
7 M. K. Smith and O. Š. Miljanić, Arylene Ethynylene Macrocycles: From Molecular Hosts to Components of High-Performance Supramolecular Architectures, *Org. Biomol. Chem.*, 2015, **13**, 7841.
8 K. Tahara and Y. Tobe, Molecular Loops and Belts, *Chem. Rev.*, 2006, **106**, 5274.
9 M. Hermann, D. Wassy and B. Esser, Conjugated Nanohoops Incorporating Donor, Acceptor, Hetero- or Polycyclic Aromatics, *Angew. Chem., Int. Ed.*, 2021, **60**, 15743.
10 Y. Segawa, A. Yagi, K. Matsui and K. Itami, Design and Synthesis of Carbon Nanotube Segments, *Angew. Chem., Int. Ed.*, 2016, **55**, 5136.
11 Q.-H. Guo, Y. Qiu, M.-X. Wang and J. F. Stoddart, Aromatic Hydrocarbon Belts, *Nat. Chem.*, 2021, **13**, 402.
12 J. S. Wössner, D. Wassy, A. Weber, M. Bovenkerk, M. Hermann, M. Schmidt and B. Esser, [*n*] Cyclodibenzopentalenes as Antiaromatic Curved Nanocarbons with High Strain and Strong Fullerene Binding, *J. Am. Chem. Soc.*, 2021, **143**, 12244.
13 D. Wassy, M. Pferifer and B. Esser, Synthesis and Properties of Conjugated Nanohoops Incorporating Dibenzo[*a*,*e*] Pentalenes: [2]DBP[12]CPPs, *J. Org. Chem.*, 2020, **85**, 34.
14 M. D. Peeks, T. D. W. Claridge and H. L. Anderson, Aromatic and Antiaromatic Ring Currents in a Molecular Nanoring, *Nature*, 2017, **541**, 200.
15 M. D. Peeks, M. Jirásek, T. D. W. Claridge and H. L. Anderson, Global Aromaticity and Antiaromaticity in Porphyrin Nanoring Anions, *Angew. Chem., Int. Ed.*, 2019, **58**, 15717.
16 M. Jirásek, H. L. Anderson and M. D. Peeks, From Macrocycles to Quantum Rings: Does Aromaticity Have a Size Limit?, *Acc. Chem. Res.*, 2021, **54**, 3241.
17 X. Lu, D. An, Y. Han, Y. Zou, Y. Qiao, N. Zhang, D. Chang, J. Wu and Y. A. Liu, Cyclopenta-Fused Dibenzo[*b*,*d*] thiophene-*co*-Phenanthrene Macrocyclic Tetraradicaloid, *Chem. Sci.*, 2021, **12**, 3952.
18 X. Lu, T. Y. Gopalakrishna, H. Phan, T. S. Herng, Q. Jiang, C. Liu, G. Li, J. Ding and J. Wu, Global Aromaticity in Macrocyclic Cyclopenta-Fused Tetraphenanthrenylene Tetraradicaloid and Its Charged Species, *Angew. Chem., Int. Ed.*, 2018, **57**, 13052.
19 H. Gregolińska, M. Majewski, P. J. Chmielewski, J. Gregoliński, A. Chien, J. Zhou, Y.-L. Wu, Y. J. Bae, M. R. Wasielewski, P. M. Zimmerman and M. Stępień, Fully Conjugated [4]Chrysaorene. Redox-Coupled Anion Binding in a Tetraradicaloid Macrocycle, *J. Am. Chem. Soc.*, 2018, **140**, 14474.
20 R. Gleiter and G. Haberhauer, *Aromaticity and Other Conjugation Effects*, Wiley-VCH Verlag GmbH & Co. KGaA, Weinheim, 2012 and references therein.
21 T. M. Krygowski, M. K. Cyrañski, Z. Czarnocki, G. Häfelinger and A. R. Katritzky, Aromaticity: A Theoretical Concept of Immense Practical Importance, *Tetrahedron*, 2000, **56**, 1783.
22 A. Minsky, A. Y. Meyer and M. Rabinovitz, Paratropicity and Antiaromaticity: Role of the HOMO–LUMO Energy Gap, *Tetrahedron*, 1985, **41**, 785.
23 R. Nozawa, H. Tanaka, W.-Y. Cha, Y. Hong, I. Hisaki, S. Shimizu, J.-Y. Shin, T. Kowalczyk, S. Irle, D. Kim and H. Shinokubo, Stacked Antiaromatic Porphyrins, *Nat. Commun.*, 2016, **7**, 13620.
24 S. Ishikawa, K. Yamasumi, S. Sugiura, S. Sato, G. Watanabe, Y. H. Koo, S. Seki, Y. Bando, Y. Haketa, H. Shinokubo and H. Maeda, Norcorroles as Antiaromatic π-Electronic Systems that Form Dimension-Controlled Assemblies, *Chem. Sci.*, 2024, **45**, 7603.
25 S.-Y. Liu, S. Li, S. Ukai, R. Nozawa, N. Fukui, R. Sugimori, R. Kishi and H. Shinokubo, Homochiral and Heterochiral Self-Sorting Assemblies of Antiaromatic Ni(II) Norcorrole Dimers, *Chem.–Eur. J.*, 2024, **30**, e202400292.
26 D. Zhao and J. S. Moore, Shape-Persistent Arylene Ethynylene Macrocycles: Synthesis and Supramolecular Chemistry, *Chem. Commun.*, 2003, 807.
27 H. Gregorius, M. Baumgarten, R. Reuter, K. Müllen and N. Tyutyulkov, *meta*-Phenylene Units as Conjugation

Barriers in Phenylenevinylene Chain, *Angew Chem. Int. Ed. Engl.*, 1992, **31**, 1653.
28 U. H. F. Bunz, Poly(aryleneethynylene)s: Syntheses, Properties, Structures, and Applications, *Chem. Rev.*, 2000, **100**, 1605.
29 K. M. Gaab, A. L. Thompson, J. Xu, T. J. Martínez and C. J. Bardeen, Meta-Conjugation and Excited-State Coupling in Phenylacetylene Dendrimers, *J. Am. Chem. Soc.*, 2003, **125**, 9288.
30 A. L. Thompson, K. M. Gaab, J. Xu, C. J. Bardeen and T. J. Martínez, Variable Electronic Coupling in Phenylacetylene Dendrimers: The Role of Förster, Dexter, and Charge-Transfer Interactions, *J. Phys. Chem. A*, 2004, **108**, 671.
31 K. Tahara, T. Yoshimura, M. Sonoda, Y. Tobe and R. V. Williams, Theoretical Studies on Graphyne Substructures: Geometry, Aromaticity, and Electronic Properties of the Multiply Fused Dehydrobenzo[12] annulenes, *J. Org. Chem.*, 2007, **72**, 1437.
32 C. R. Arroyo, S. Tarkuc, R. Frisenda, J. S. Seldenthuis, C. H. M. Woerde, R. Eelkema, F. C. Grozema and H. S. J. van der Zant, Signatures of Quantum Interference Effects on Charge Transport Through a Single Benzene Ring, *Angew. Chem., Int. Ed.*, 2013, **52**, 3152.
33 R. K. Singh and M. K. Mishra, Investigation of Ethynylpyridines Using the Electron Propagator Theory, *Int. J. Quantum Chem.*, 2012, **112**, 426.
34 C. A. Johnson II, B. A. Baker, O. B. Berryman, L. N. Zakharov, M. J. O'Connor and M. M. Haley, Synthesis and Characterization of Pyridine- and Thiophene-Based Platinacyclynes, *J. Organomet. Chem.*, 2006, **691**, 413.
35 J. Krömer, I. Rios-Carreras, G. Fuhrmann, C. Musch, M. Wnderlin, T. Devaerdemaeker, E. Mena-Osteritz and P. Bäuerle, Synthesis of the First Fully α-Conjugated Macrocyclic Oligothiophenes: Cyclo[*n*]Thiophenes with Tunable Cavities in the Nanometer Regime, *Angew. Chem., Int. Ed.*, 2000, **39**, 3481.
36 K. Nakao, M. Nishimura, T. Tamachi, Y. Kuwatani, H. Miyasaka, T. Nishinaga and M. Iyoda, Giant Macrocycles Composed of Thiophene, Acetylene, and Ethylene Building Blocks, *J. Am. Chem. Soc.*, 2006, **128**, 16740.
37 C.-Y. Kwong, M. Leung, S.-C. Lin, T.-L. Chan and H.-F. Chow, Synthesis and Characterization of Oligo(2,7-biphenylenylene-(*E*)-vinylene)s, *Tetrahedron Lett.*, 1996, **37**, 5913.
38 M. Gantenbein, X. Li, S. Sangtarash, J. Bai, G. Olsen, A. Alqorashi, W. Hong, C. J. Lambert and M. R. Bryce, Exploring Antiaromaticity in Single-Molecule Junctions Formed from Biphenylene Derivatives, *Nanoscale*, 2019, **11**, 20659.
39 W. C. Lothrop, Biphenylene, *J. Am. Chem. Soc.*, 1941, **63**, 1187.
40 S. Radenković, J. Tošović, R. W. A. Havenith and P. Bultinck, Ring Currents in Benzo- and Benzocyclobutadieno-Annelated Biphenylene Derivatives, *ChemPhysChem*, 2015, **16**, 216.
41 N. Verdal and B. S. Hudson, Inelastic Neutron Scattering and Periodic DFT Studies of Crystalline Aromatic Materials: Biphenylene—A Mills–Nixon Molecule, *Chem. Phys. Lett.*, 2007, **434**, 241.
42 S. M. Bachrach, On the Destabilization (Strain) Energy of Biphenylene, *J. Phys. Chem. A*, 2008, **112**, 7750.
43 N. Lin, H. Solheim, X. Zhao, F. Santoro and K. Ruud, First Principles Studies of the Vibrationally Resolved Magnetic Circular Dichroism Spectra of Biphenylene, *J. Chem. Theory Comput.*, 2013, **9**, 1557.
44 Q. Fan, L. Yan, M. W. Tripp, O. Krejčí, S. Dimosthenous, S. R. Kachel, M. Chen, A. S. Foster, U. Koert, P. Liljeroth and J. M. Gottfried, Biphenylene Network: A Nonbenzenoid Carbon Allotrope, *Science*, 2021, **372**, 852.
45 Z. Rashid, J. H. van Lenthe and R. W. A. Havenith, Resonance and Aromaticity: An *Ab Initio* Valence Bond Approach, *J. Phys. Chem. A*, 2012, **116**, 4778.
46 H. Kiliç and M. Balci, A New Antiaromatic Compound: 1,4-Biphenylenequinone Synthesis and Trapping Reactions: Can a Quinone Unit Stabilize the Cyclobutadiene?, *Tetrahedron*, 2001, **57**, 9889.
47 D. Asai and K. Tahara, Synthesis and Reactivity of an X-Shaped Molecule: Reversible Formation and Cleavage of a Four-Membered Ring in Response to External Stimuli, *Org. Lett.*, 2024, **26**, 4898.
48 S. Toyota, Rotational Isomerism Involving Acetylene Carbon, *Chem. Rev.*, 2010, **110**, 5398.
49 K. Honda and K. Tahara, Heptagonal Molecular Tiling *via* Self-Assembly of Heptagonal Phenylene-Ethynylene Macrocycle at the Liquid–Solid Interface, *Chem.–Eur. J.*, 2024, **30**, e202400926.
50 J. Rissler, Effective Conjugation Length of π-Conjugated System, *Chem. Phys. Lett.*, 2004, **395**, 92.
51 H. Matsuki, K. Okubo, Y. Takaki, Y. Niihori, M. Mitsui, E. Kayahara, S. Yamago and K. Kobayashi, Synthesis and Properties of a Cyclohexa-2,7-anthrylene Ethynylene Derivative, *Angew. Chem., Int. Ed.*, 2021, **60**, 998.
52 S. Toyota, H. Miyahara, M. Goichi, S. Yamasaki and T. Iwanaga, Chemistry of Anthracene-Acetylene Oligomers. XIII. Synthesis, Structures, and Spectroscopic Properties of All Possible 1,8-Anthrylene Cyclic Tetramers with Acetylene and Diacetylene Linkers, *Bull. Chem. Soc. Jpn.*, 2009, **82**, 931.
53 Y. Tobe, N. Utsumi, K. Kawabata, A. Nagano, K. Adachi, S. Araki, M. Sonoda, K. Hirose and K. Naemura, *m*-Diethynylbenzene Macrocycles: Synthesis and Self-Association Behavior in Solution, *J. Am. Chem. Soc.*, 2002, **124**, 5350.
54 Z. Luo, X. Yang, K. Cai, X. Fu, D. Zhang, Y. Ma and D. Zhao, Toward Möbius and Tubular Cyclopolyarene Nanorings *via* Arylbutadiyne Macrocycles, *Angew. Chem., Int. Ed.*, 2020, **59**, 14854.
55 L. Zhang, H. Gopee, D. L. Hughes and A. N. Cammidge, Antiaromatic Twinned Triphenylene Discotics Showing Nematic Phases and 2-Dimensional π-Overlap in the Solid State, *Chem. Commun.*, 2010, **46**, 4255.
56 K. B. Wiberg, Application of the Pople-Santry-Segal CNDO Method to the Cyclopropylcarbinyl and Cyclobutyl Cation and to Bicyclobutane, *Tetrahedron*, 1968, **24**, 1083.

57 H. L. Schmider and A. D. Becke, Chemical Content of the Kinetic Energy Density, *J. Mol. Struct.:THEOCHEM*, 2000, **527**, 51.
58 S. N. Steinmann, Y. Mo and C. Corminboeuf, How Do Electron Localization Functions Describe π-Electron Delocalization?, *Phys. Chem. Chem. Phys.*, 2011, **13**, 20584.
59 K. Kaiser, L. M. Scriven, F. Schulz, P. Gawel, L. Gross and H. L. Anderson, An Sp-Hybridized Molecular Carbon Allotrope, Cyclo[18]Carbon, *Science*, 2019, **365**, 1299.
60 G. V. Baryshnikov, R. R. Valiev, A. V. Kuklin, D. Sundholm and H. Ågren, Cyclo[18]carbon: Insight into Electronic Structure, Aromaticity, and Surface Coupling, *J. Phys. Chem. Lett.*, 2019, **10**, 6701.
61 P. von R. Schleyer, C. Maerker, A. Dransfeld, H. Jiao and N. J. R. van Eikema Hommes, Nucleus-Independent Chemical Shifts: A Simple and Efficient Aromaticity Probe, *J. Am. Chem. Soc.*, 1996, **118**, 6317.
62 H. Fallah-Bagher-Shaidaei, C. S. Wannere, C. Corminboeuf, R. Puchta and P. von R. Schleyer, Which NICS Aromaticity Index for Planar π Rings Is Best?, *Org. Lett.*, 2006, **8**, 863.
63 J. Jusélius, D. Sundholm and J. Gauss, Calculation of Current Densities Using Gauge-Including Atomic Orbitals, *J. Chem. Phys.*, 2004, **121**, 3952.
64 H. Fliegl, S. Taubert, O. Lehtonen and D. Sundholm, The Gauge-including Magnetically Induced Current Method, *Phys. Chem. Chem. Phys.*, 2011, **13**, 20500.
65 S. Taubert, D. Sundholm, J. Jusélius, W. Klopper and H. Fliegl, Calculation of Magnetically Induced Currents in Hydrocarbon Nanorings, *J. Phys. Chem. A*, 2008, **112**, 13584.
66 R. Herges and D. Geuenich, Delocalization of Electrons in Molecules, *J. Phys. Chem. A*, 2001, **105**, 3214.
67 D. Geuenich, K. Hess, F. Köhler and R. Herges, Anisotropy of the Induced Current Density (ACID), a General Method to Quantify and Visualize Electronic Delocalization, *Chem. Rev.*, 2005, **105**, 3758.
68 D. P. Goronzy, M. Ebrahimi, F. Rosei, Arramel, Y. Fang, S. De Feyter, S. L. Tait, C. Wang, P. H. Beton, A. T. S. Wee, P. S. Weiss and D. F. Perepichka, Supramolecular Assemblies on Surfaces: Nanopatterning, Functionality, and Reactivity, *ACS Nano*, 2018, **12**, 7445.
69 J. A. Elemans, S. Lei and S. De Feyter, Molecular and Supramolecular Networks on Surfaces: From Two-Dimensional Crystal Engineering to Reactivity, *Angew. Chem., Int. Ed.*, 2009, **48**, 7298.
70 Y. Tobe, K. Tahara and S. De Feyter, Adaptive Building Blocks Consisting of Rigid Triangular Core and Flexible Alkoxy Chains for Self-Assembly at Liquid/Solid Interfaces, *Bull. Chem. Soc. Jpn.*, 2016, **89**, 1277.
71 X. Zhang, Q. D. Zeng and C. Wang, Host-Guest Supramolecular Chemistry at Solid-Liquid Interface: An Important Strategy for Preparing Two-Dimensional Functional Nanostructures, *Sci. China: Chem.*, 2014, **57**, 13.
72 K. Tahara, S. Furukawa, H. Uji-i, T. Uchino, T. Ichikawa, J. Zhang, W. Mamdouh, M. Sonoda, F. C. De Schryver, S. De Feyter and Y. Tobe, Two-Dimensional Porous Molecular Networks of Dehydrobenzo[12]annulene Derivatives *via* Alkyl Chain Interdigitation, *J. Am. Chem. Soc.*, 2006, **128**, 16613.
73 K. Tahara, T. Balandina, S. Furukawa, S. De Feyter and Y. Tobe, Molecular Pentagonal Tiling: Self-Assemblies of Pentagonal-Shaped Macrocycles at Liquid/Solid Interface, *CrystEngComm*, 2011, **13**, 5551.
74 S.-S. Jester, E. Sigmund and S. Höger, Nanopatterning by Molecular Polygons, *J. Am. Chem. Soc.*, 2011, **133**, 11062.
75 J. P. Rabe and S. Buchholz, Commensurability and Mobility in Two-Dimensional Molecular Patterns on Graphite, *Science*, 1991, **253**, 424.
76 R. Lazzaroni, A. Calderone, G. Lambin, J. P. Rabe and J. L. Brédas, A Theoretical Approach to the STM Imaging of Adsorbates on the Graphite Surface, *Synth. Met.*, 1991, **41**, 525.
77 A. J. Groszek, Selective Adsorption at Graphite/Hydrocarbon Interfaces, *Proc. R. Soc. London, Ser. A*, 1970, **314**, 473.
78 F. Jäckel, M. D. Watson, K. Müllen and J. P. Rabe, Tunneling through Nanographene Stacks, *Phys. Rev. B: Condens. Matter Mater. Phys.*, 2006, **73**, 045423.
79 F. Jäckel, M. Ai, J. Wu, K. Müllen and J. P. Rabe, Solvent Molecules in an Epitaxially Grown Scaffold of Star-Shaped Nanographenes, *J. Am. Chem. Soc.*, 2005, **127**, 14580.
80 S.-S. Jester, A. V. Aggarwal, D. Kalle and S. Höger, Mono- and multilayers of Molecular Spoked Carbazole Wheels on Graphite, *Beilstein J. Org. Chem.*, 2014, **10**, 2793.
81 S. Lee, B. E. Hirsch, Y. Liu, J. R. Dobscha, D. W. Burke, S. Tait and A. H. Flood, Multifunctional Tricarbazolo Triazolophane Macrocycles: One-Pot Preparation, Anion Binding, and Hierarchical Self-Organization of Multilayers, *Chem.–Eur. J.*, 2016, **22**, 560.
82 B. Venkataraman, J. J. Breen and G. W. Flynn, Scanning Tunneling Microscopy Studies of Solvent Effects on the Adsorption and Mobility of Triacontane/Triacontanol Molecules Adsorbed on Graphite, *J. Phys. Chem.*, 1995, **99**, 6608.
83 C. Bannwarth, E. Caldeweyher, S. Ehlert, A. Hansen, P. Pracht, J. Seibert, S. Spicher and S. Grimme, Extended Tight-Binding Quantum Chemistry Methods, *Wiley Interdiscip. Rev.: Comput. Mol. Sci.*, 2020, **11**, e01493.
84 S. Grimme, C. Bannwarth and P. Shushkov, A Robust and Accurate Tight-Binding Quantum Chemical Method for Structures, Vibrational Frequencies, and Noncovalent Interactions of Large Molecular Systems Parameterized for All spd-Block Elements (Z = 1–86), *J. Chem. Theory Comput.*, 2017, **13**, 1989.
85 N. Tchebotareva, X. Yin, M. D. Watson, P. Samorì, J. P. Rabe and K. Müllen, Ordered Architectures of a Soluble Hexa-*peri*-hexabenzocoronene–pyrene Dyad: Thermotropic Bulk Properties and Nanoscale Phase Segregation at Surfaces, *J. Am. Chem. Soc.*, 2003, **125**, 9734.
86 A. Miura, Z. Chen, H. Uji-i, S. De Feyter, M. Zdanowska, P. Jonkheijm, A. P. H. J. Schenning, E. W. Meijer, F. Würthner and F. C. De Schryver, Bias-Dependent Visualization of Electron Donor (D) and Electron Acceptor (A) Moieties in a Chiral DAD Triad Molecule, *J. Am. Chem. Soc.*, 2003, **125**, 14968.